

The Relevance of Measurement Systems Analysis

A Procter & Gamble Case Study on MSA Methodology and Applications

DATE

**OCTOBER
10 AND 12**

TIME

**16:00 CET,
10 am EST**



**CHRISTIAN
NEU**

Scientist
Procter & Gamble



**JERRY
FISH**

Systems Engineer
JMP



**JASON
WIGGINS**

Senior Systems
Engineer
JMP

[Register now](#)

Electrochemically Driven Assembly of Chitosan Hydrogels on PEDOT Surfaces

Aruã Clayton Da Silva,* Celine Amadou-Douah, Stavriani Koiliari, Jinfei Du, Riya K. K. Chauhan, Thomas Edward Paterson, and Ivan Rusev Minev*

Hydrogels are attracting interest in the field of bioelectronics due to their ability to serve as coatings on electrodes, improving the electrochemical interface, addressing the mechanical mismatch, and offering potential for localized drug or cell delivery. Challenges persist in integrating hydrogels with electrodes typically composed of metals and/or organic semiconductors. Here, an electrochemically driven method is introduced for direct growth of chitosan hydrogels onto poly(3,4-ethylenedioxythiophene) (PEDOT) surfaces. The growth of ionic gelation chitosan is triggered by electrical release of a specific dopant, tripolyphosphate (TPP), from PEDOT. As a result, chitosan hydrogels grow directly from the PEDOT surface and firmly attach to it. Although this process temporarily reduces PEDOT to the benzoid structure, its unique electroactivity allows for reversible conversion to the quinoid structure after chitosan hydrogel assembly. Once assembled, the chitosan hydrogel coating can be further functionalized. The introduction of covalent cross-links and incorporation of additional interpenetrating polymer networks (IPNs) are explored. Electrochemical characterization reveals that an interface with favorable properties is formed between PEDOT and ionic-covalent chitosan, functionalized with a PEDOT IPN. The electroactivity of the proposed method surpasses any other PEDOT/chitosan system reported in the literature. These results underscore the potential of this material for bioelectronics applications.

1. Introduction

Traditional microelectronic systems constructed with hard and dry technological materials are challenging to interface with soft, wet, and living tissues.^[1] A promising solution utilizes soft hydrogels as a bridge between the soft and rigid systems.^[2] This has been explored in the context of implantable neural probes where the electrodes are coated with a soft hydrogel.^[3,4] Such coatings have the capacity to reduce the mechanical mismatch between soft neural tissues and rigid materials (metals, silicon, or organic conductors) used to construct electrodes.^[5] Hydrogel coatings can improve the electrical properties of the interface by reducing impedance and increasing the charge injection capacity.^[6-8] The hydrogel coating may support the release of therapeutic agents such as neurotrophin or dexamethasone.^[9,10] Encapsulation of living cells in the coating may enable reduction of fibrotic scars forming around the electrode.^[11,12] The realization of these advantageous features is challenging because it requires the integration of

A. C. Da Silva, C. Amadou-Douah, S. Koiliari, T. E. Paterson, I. R. Minev
Department of Automatic Control and Systems Engineering
Faculty of Engineering
University of Sheffield
Mappin Street, Sheffield S1 3JD, UK
E-mail: a.dasilva@sheffield.ac.uk; minev@ipfdd.de


A. C. Da Silva, J. Du
Insigneo Institute for in silico Medicine
University of Sheffield
Pam Liversidge Building, Sheffield S1 3JD, UK

J. Du
Department of Chemical and Biological Engineering
Faculty of Engineering
University of Sheffield
Mappin Street, Sheffield S1 4LZ, UK

R. K. K. Chauhan
Department of Bioengineering
Faculty of Engineering
University of Sheffield
Sheffield S1 3JD, UK

T. E. Paterson
Department of Mechanisms of Health and Disease
School of Clinical Dentistry
University of Sheffield
19 Claremont Crescent, Sheffield S10 2TA, UK

I. R. Minev
Institute of Biofunctional Polymer Materials
Leibniz Institute of Polymer Research Dresden
Hohe Str. 6, 01069 Dresden, Germany

 The ORCID identification number(s) for the author(s) of this article can be found under <https://doi.org/10.1002/mame.202300263>

© 2023 The Authors. Macromolecular Materials and Engineering published by Wiley-VCH GmbH. This is an open access article under the terms of the Creative Commons Attribution License, which permits use, distribution and reproduction in any medium, provided the original work is properly cited.

DOI: 10.1002/mame.202300263

materials with different elemental compositions leading to orders of magnitude differences in elastic moduli, hydration, and swelling.^[13] Several approaches have been developed to facilitate the attachment of hydrogels to dissimilar rigid materials such as metals. These typically rely on engineering the nanostructure at the interface that prevents the propagation of microcracks responsible for delamination.^[14,15] Coating a rigid surface with a hydrogel can be achieved in different ways, for example, by pouring precursor solutions on a prepared surface and applying triggers to cross-link the final material or by lamination of preformed films.^[16,17] Electrochemical methods have also been employed for growing hydrogels directly on conductive surfaces.^[18–22] These methods have the advantage that gelation occurs only over the conductive surface (conformal coating), the rate of gelation can be potentiostatically controlled and interfaces with a smooth transition zone can be formed.^[7,23]

In the context of electrodes, the electrical interface between hydrogel and rigid (conductive) substrate is of key importance. This is challenging to achieve because hydrogels typically are ionic conductors while metals are electronic conductors. This may be addressed by functionalizing already formed hydrogel coatings to have dual electronic-ionic conductivity, thus enhancing the charge transfer across the soft-rigid interface.^[24] A number of approaches to enhance the conductivity of hydrogels have been reported. These include incorporation of metallic additives or interpenetrating networks (IPNs) of conductive polymer.^[25–27] Among the conducting polymers, PEDOT is a promising candidate due to its good electronic/ionic conductivity, biocompatibility, and processability via physical dispersion, oxidative reactions, or electropolymerization within the hydrogel.^[28–32]

The hydrogel coating may be selected among various natural or synthetic polymers. Natural polysaccharides (alginate, cellulose, hyaluronic acid, gelatin, chitosan, and others) are frequently used to create hydrogels due to their excellent biocompatibility and biodegradability.^[33,34] For instance, chitosan is a hydrogel extensively applied for drug delivery or adhesive wound-dressing applications.^[35,36] Additionally, it has attracted attention also in bioelectronics for its ability to conduct protons.^[37] Chitosan hydrogels can be assembled by ionic, covalent cross-linking or by precipitation.^[38–41] Ionically cross-linked chitosan, mostly uses the triphosphosphate (TPP) anion as cross-linker.^[42] Chitosan hydrogels are rarely processed as conformal coatings, for example, self-assembled chitosan-TPP gels typically form in spherical morphology, as beads, microparticles, or nanoparticles.^[43–46]

In this study, we developed a novel approach wherein chitosan hydrogels are grown directly on PEDOT, which is electropolymerized on the surface of gold and platinum wires. The uniqueness of our approach lies in achieving the direct growth of chitosan hydrogel onto PEDOT using an electrochemical–chemical (EC) mechanism. Here, TPP is introduced into the PEDOT polymer matrix as dopant, triggering the ionic gelation of chitosan upon electrical release. This EC mechanism enables precise and controllable electrical gelation of the hydrogel. Our primary objective was to achieve successful integration of the two components in the core–shell hydrogel, emphasizing the ability to control the electro-assisted assembly of the chitosan hydrogel and optimize the electrode coatings. Postassembly modifications, including covalent cross-links and IPNs, were explored to further enhance the electrochemical performance of the system. With this, we

aim to develop a functionalized conductive hydrogel encompassing enhanced conductivity and improved integration to the electrode surface. The PEDOT-hydrogel interface was assessed using electrochemical techniques, such as cyclic voltammetry (CV) and electrochemical impedance spectroscopy (EIS), revealing superior electrochemical performance compared with previously reported PEDOT/chitosan systems. This study highlights the immense potential of the proposed material for bioelectronics applications.

2. Results and Discussions

2.1. Formation of PEDOT/Chitosan Hydrogels

We start by exploring if electro-assisted cross-linking of chitosan can offer a potentiostatically controlled way to assemble adherent hydrogels on PEDOT surfaces. We first polymerized PEDOT in the presence of the doping agent (TPP) (**Figure 1a**, steps 1 & 2).

The schematic in **Figure 1a** shows the chemical reaction steps: (1) the electropolymerization of EDOT monomers at +1.2 V to form PEDOT chains (initially in neutral state, benzoid structure) followed by (2) the oxidation and doping of the PEDOT by the anion TPP (generating positive charges in the PEDOT and quinoid structure). Here, we used a pulsed electropolymerization method where the potential at the working electrode (WE) is held at oxidative potentials (+1.2 V vs AgAg/Cl) for a brief time (0.5 s), followed by holding it at the open-circuit potential (OCP) for interpulse periods lasting 5 s. As reported previously, this method allows time for diffusion and thus for more efficient doping of PEDOT.^[7] The PEDOT:TPP-coated wire is then transferred to a chitosan solution and in step (3) PEDOT is reduced at –1.2 V, releasing the TPP dopant to cross-link the chitosan hydrogel. **Figure 1b** illustrates steps in the gel formation that correspond to the chemical reactions described in **Figure 1a**. The chitosan coatings produced in this way are ionically cross-linked and will be referred to as i-C gels.

2.2. Electro-Assisted Cross-Linking of PEDOT/Chitosan Hydrogels

The deposition and characterization of PEDOT:TPP and i-C gels is presented in **Figure 2**. **Figure 2a** shows an amperogram obtained during deposition of PEDOT:TPP. The potential of +1.2 V was selected for electropolymerization that was based on the observation of a CV peak for this process (**Figure S1**, Supporting Information). **Figure 2b** shows a typical amperogram recorded during reduction of PEDOT:TPP. We applied –1.2 V for 600 s to ensure the whole PEDOT film was reduced and all TPP molecules have been released in the chitosan solution. **Figure 2c** shows photographs of the PEDOT:TPP and i-C gels grown around a gold wire. The pulsed electropolymerization method generates PEDOT:TPP coatings with a rough surface morphology, enabling higher doping of the structure as compared with smooth coatings.^[7] The chitosan hydrogel fully envelops the PEDOT creating a smooth outer surface. The adherent coating of i-C produced by our electro-assisted method is in contrast with the microspheres typically observed with

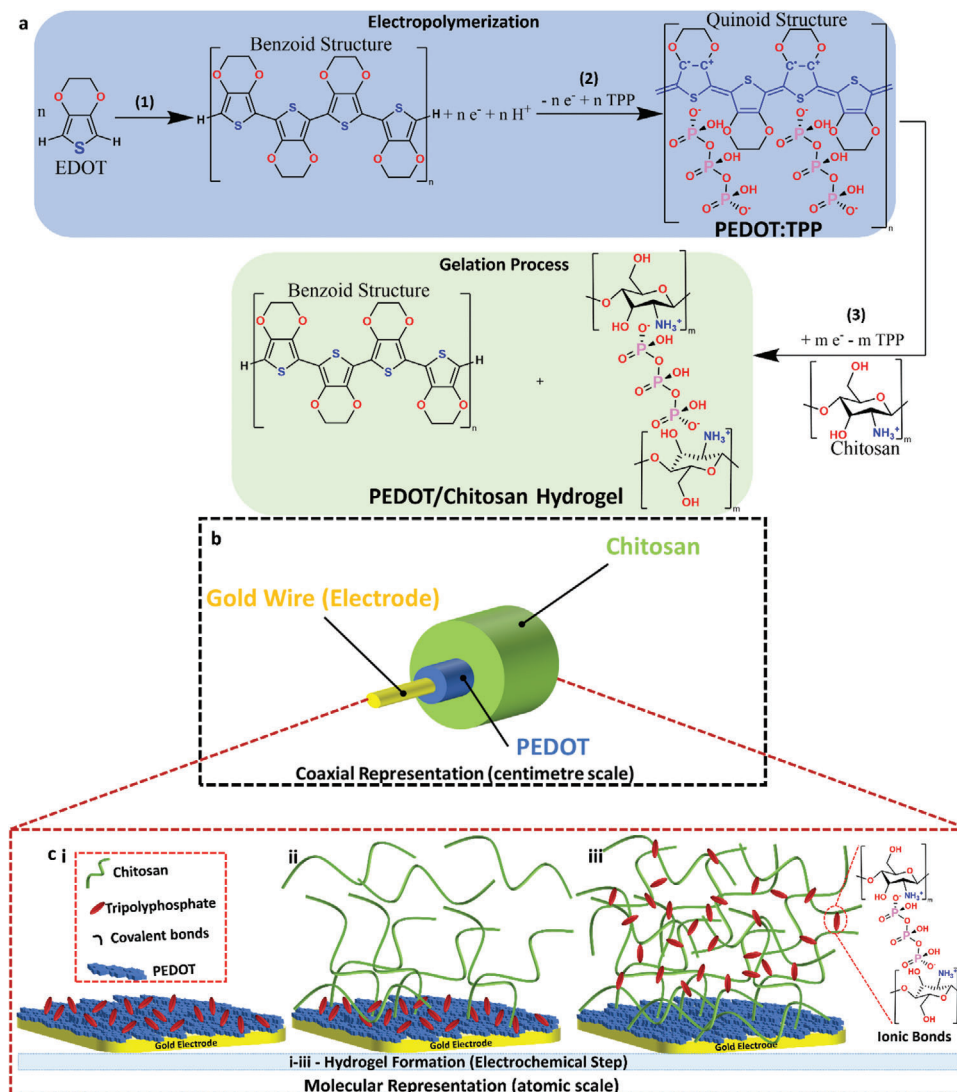


Figure 1. a) Chemical reactions of the (1) electropolymerization of EDOT to PEDOT followed by (2) oxidation of PEDOT polymer from neutral form (benzoid structure) to oxidized form (bipolaron, quinoid structure) doped with TPP anion (+1.2 V, pulsed method). In a subsequent step (3), electrical release of TPP ions (−1.2 V for 20 min) assembles the chitosan biomacromolecules as an ionically cross-linked hydrogel. b) Coaxial representation (black dashed square) of the core–shell structures deposited over gold wire. c) Molecular representation (dark red dashed square) of the hydrogel formation as (i) the PEDOT:TPP, (ii) PEDOT:TPP in solution containing chitosan biomacromolecules, and (iii) PEDOT/chitosan hydrogel ionically cross-linked (by TPP ions).

chitosan hydrogels cross-linked with TPP.^[47–50] We were able to create a PEDOT/i-C hydrogel on different conductive substrates by using a combination of electrodeposition and electro-assisted assembly. To illustrate this approach, we also electrodeposited the hydrogel onto a PtIr wire microelectrode ($d = 100 \mu\text{m}$) under two different electrodeposition charges (Figure S2, Supporting Information). Figure 2d shows a table summarizing key growth parameters obtained from amperograms. We determined the electropolymerization charge ($Q_{\text{electropolymerization}}$), which enabled us to calculate the effective surface coverage (Γ_{PEDOT}) for the PEDOT film. From the reduction charge of PEDOT:TPP ($Q_{\text{reduction}}$), we estimated the doping level of PEDOT:TPP ($\approx 22\%$) and the amount of TPP released ($5.9 \pm 1.5 \mu\text{mol}$). Figure 2e shows typical CV of PEDOT:TPP (as prepared) and PEDOT/i-C

(as prepared) coatings immersed in phosphate buffer saline (PBS) media (both formed by 1000 pulses). We observed that the PEDOT/i-C interface had a slightly better electroactivity as indicated by higher currents in the CV. Figure 2f presents typical EIS results from PEDOT/i-C structures in pristine form (as prepared, just after chitosan formation) and following cycling in PBS. In as-prepared structures, it is presumed the PEDOT film is fully reduced following loss of TPP, while following ten cycles, PEDOT has been redoped by anions recruited from the PBS electrolyte. This is supported by the observation of large differences in the corresponding Nyquist plots. The reduced PEDOT presents two semicircles, suggesting the resistances of the PEDOT film (smaller, higher frequencies) and the chitosan hydrogel (bigger, lower frequencies) are not electronically

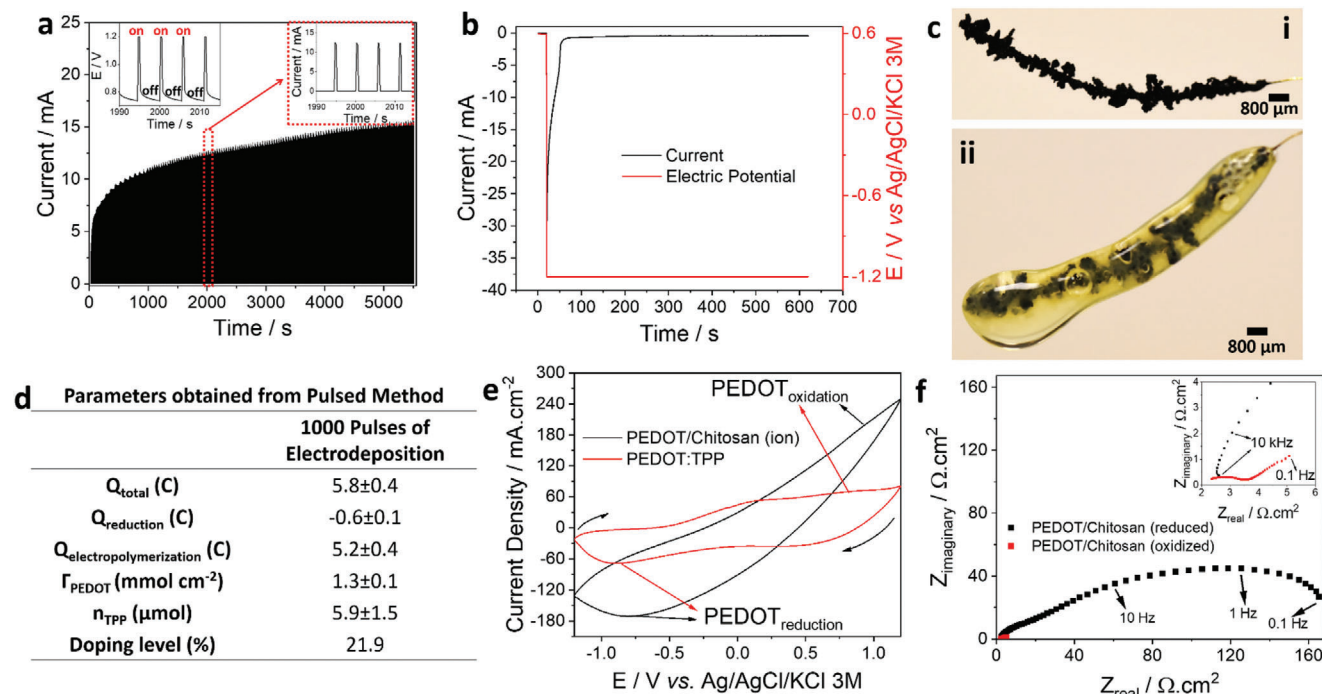


Figure 2. a) Chronoamperometry (CA) profile of pulsed method for 1000 electropolymerization pulses to obtain PEDOT:TPP. Electric potential versus time (inset left) and current versus time (inset right) showing in details a sequence of four pulses. b) CA profile (step potential) at -1.2 V for 600 s of PEDOT reduction (TPP release) ionically cross-linking the chitosan hydrogel. c) Photographs of the PEDOT:TPP coating (i) and PEDOT/i-C core-shell structures (ii). d) Table containing growth parameters obtained from the electropolymerization and electro-assisted cross-linking. e) CV of the PEDOT:TPP (red line) and PEDOT/i-C gel (black line) in PBS media at 100 mV s⁻¹. f) Nyquist plot of the EIS for the PEDOT/i-C gel with PEDOT in reduced state (at end of gelation, black) and after ten cycles (redoped, red) in PBS media.

integrated. The oxidized PEDOT (after cycling in PBS) shows significantly reduced resistance and a single semicircle, suggesting PEDOT and chitosan hydrogel are electronically integrated in a more conductive interface. While the gelation process temporarily reduces PEDOT to the benzoid structure, the reversible electroactivity of PEDOT allows for the conversion back to the quinoid structure after chitosan hydrogel assembly, recovering its enhanced conductivity. Additionally, as already discussed the quinoid structure of PEDOT (oxidized) is more conductive by itself, enabling electron interchain hopping and may help the integration of the electrical properties of the hydrogel.^[51,52]

2.3. Morphological and Elemental-Mapping Analysis

In order to investigate the microstructure and elemental distribution within the PEDOT and i-C compartments, we conducted SEM-EDS analysis, as shown in **Figure 3**. The PEDOT/i-C coating can be removed from the gold wire (Figure S3, Supporting Information). The removal of the PEDOT/Chitosan coating from the gold wire may introduce some microcracks to the PEDOT polymer. Nonetheless, the chitosan hydrogel plays a crucial role in providing necessary mechanical support, given the inherent brittle nature of the PEDOT polymer. The primary focus of our method is electro-assisted assembly of PEDOT/Chitosan hydrogel coatings at the electrode surface, rather than fabrication of “self-standing” structures. As illustrated in the electron micrographs in Figure 3a, the PEDOT coating has a globular fractal-

like structure, while i-C being a hydrogel is highly porous. Furthermore, we imaged transverse cross-sections that allowed us to observe the interface between PEDOT and i-C (Figure 3b). Mapping of sulfur reveals the presence of PEDOT, while phosphorus is associated with the presence of TPP. Elemental mapping shows that sulfur is predominantly found in the PEDOT coating with exception of grains that we believe were cleaved and scattered during sample preparation. As expected, we observed no phosphorus signal in the PEDOT zone, while the i-C gel zone showed a observably stronger phosphorus signal. This supports our hypothesis that during gelation, TPP is expelled from PEDOT and serves to ionically cross-link the chitosan hydrogel.^[53,54]

2.4. Functionalization of Chitosan Hydrogel Coatings

Next, we investigated if the chitosan coatings are amenable to postprocessing following initial deposition. This may be useful for engineering additional properties in the hydrogel such as dual (electronic-ionic) conductivity or potentially mechanical toughness via introduction of covalent cross-links. We modified i-C hydrogels by covalently cross-linking them (using formaldehyde) and/or forming an IPN of PEDOT within the bulk of the chitosan coating (**Figure 4**). Figure 4a provides a schematic representation of the covalent modification, which we refer to as covalent/ionic-Chitosan (ci-C) and the hydrogels modified with an IPN of PEDOT. As illustrated in Figure 4b, we further distinguish between chitosan hydrogels with oxidative formed PEDOT (ox-IPN) and

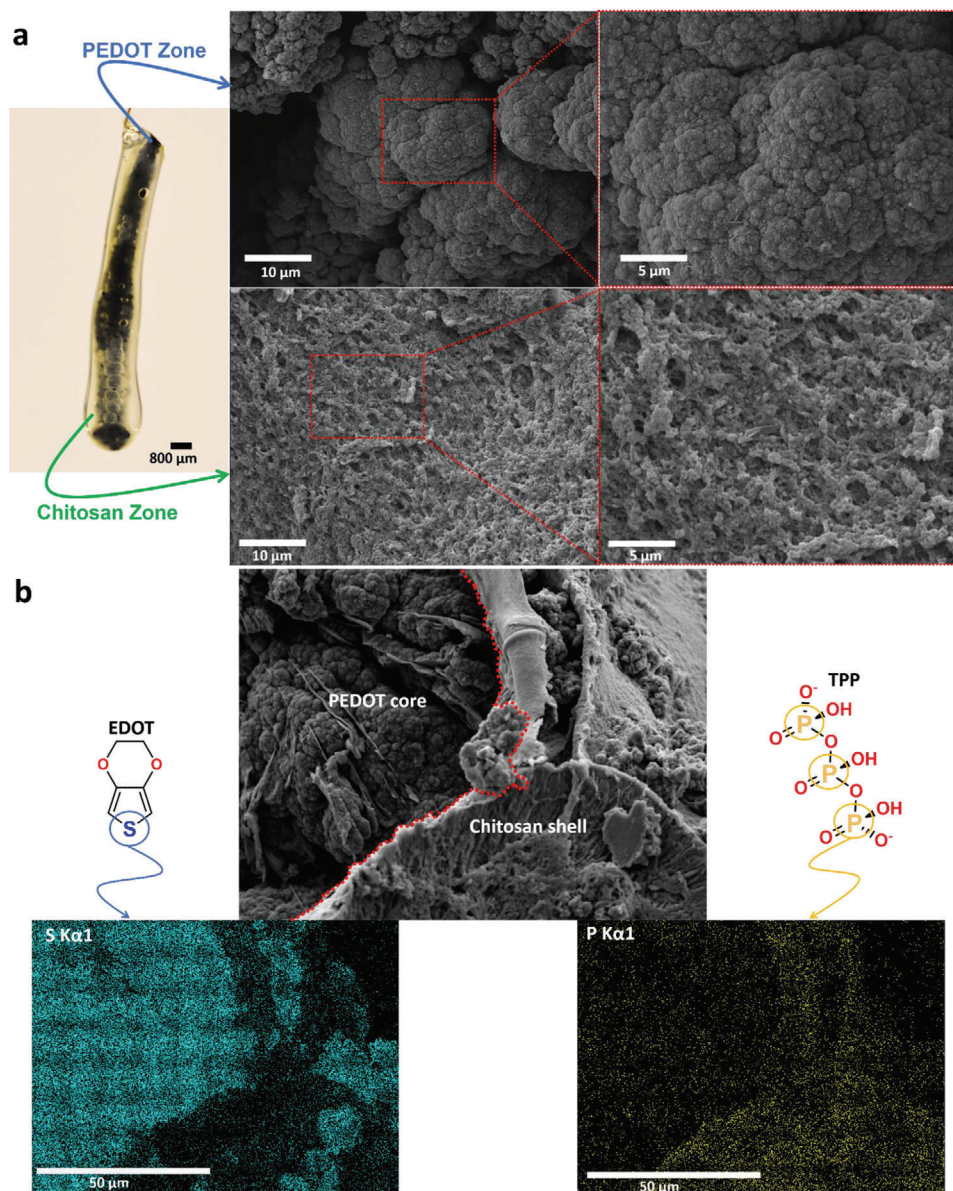


Figure 3. a) Picture of the PEDOT/i-C gel (left) highlighting the SEM images of PEDOT (top) and chitosan (bottom) areas in different magnifications. b) Transverse cross-section showing the interface (red dotted line) between PEDOT and chitosan hydrogel. The bottom insets show elemental mapping of sulfur and phosphorus.

electropolymerized PEDOT (e-IPN). In the ox-IPN method, PEDOT polymerization starts at the interface between the chitosan hydrogel and mineral oil (Figure 4b, top). The conducting polymer chain grows from outside toward the core of the hydrogel. In the e-IPN method, the conducting polymer chains grow from the solid PEDOT core toward the periphery (Figure 4b, bottom). Figure 4c shows typical EDS spectra for all types of material including as-prepared PEDOT:TPP films, nonfunctionalized (i-C) hydrogel controls and the functionalized chitosan hydrogel coatings. For all samples, we registered the EDS spectrum at locations within the PEDOT core and within the surrounding hydrogel (shown in Figure S4, Supporting Information). As expected, the EDS spectra show a higher sulfur signal in both IPN hydro-

gel coatings (ox-IPN and e-IPN) compared with pure chitosan coatings. Additionally, we observe higher intensity for phosphorus (related to TPP) in ionically cross-linked (i-C) and dual cross-linked (ci-C) chitosan than any of the IPN coatings.

2.5. Electroactivity of the PEDOT/Chitosan Interface

We investigated the electrochemical properties of the interface formed by the PEDOT core and the various chitosan-based coatings (Figure 5). Figure 5a shows CV of the i-C and ci-C coatings. The covalently functionalized hydrogel presents slightly better electroactivity. Figure 5b,c shows the effect of IPN functional-

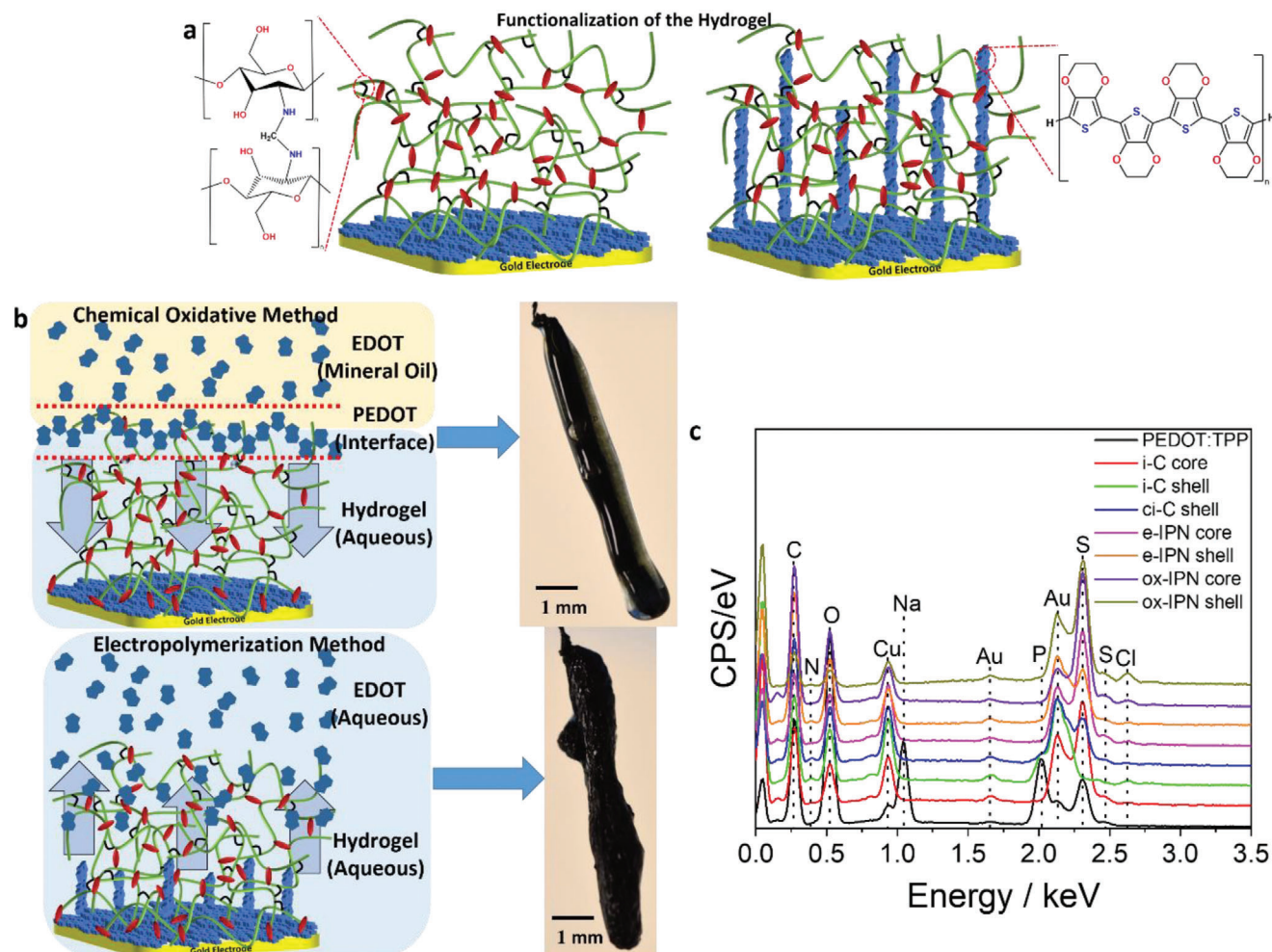


Figure 4. a) Schematic representation of the hydrogel functionalization with dually cross-linked chitosan (ionically + covalently cross-linked, left) (ci-C) and PEDOT/chitosan IPN hydrogel (right). b) Schematic representation of the two main approaches to produce an IPN (left): chemical oxidative (top, ox-IPN) and electropolymerization (bottom, e-IPN) methods. Representative picture of the conductive hydrogels after the IPN functionalization (right). c) EDS spectra indicating the elements present in the samples of PEDOT:TPP (control, black), PEDOT/i-C in the PEDOT core (i-C core, red) and chitosan gel (i-C shell, green) zones, PEDOT/ci-C in the chitosan zone (ci-C shell, blue), PEDOT/e-IPN in the PEDOT (e-IPN core, pink) and chitosan (e-IPN shell, orange) zones and PEDOT/ox-IPN in the PEDOT (ox-IPN core, purple) and chitosan (ox-IPN shell, dark yellow) zones.

ization of the i-C and ci-C coatings, respectively. Regarding the e-IPN, we found that 500 and 1000 pulses resulted in IPN that was maintained within the chitosan matrix. However, with 2000 pulses, electrodeposition of PEDOT extended outside the chitosan hydrogel (Figure S5, Supporting Information). For the ionically cross-linked hydrogel coating (i-C), the ox-IPN did not promote a well-formed IPN as evidenced by low current density (orange line). On the other hand, the current density of e-IPN samples increased as a function of the number of polymerization pulses. For the covalently cross-linked hydrogel coating (ci-C), the ox-IPN performed better, where it achieves an electroactivity similar to that of e-IPN formed by 1000 electropolymerization pulses (Figure 5c). The e-IPN did not significantly improve the electroactivity of the hydrogels until 500 pulses are applied, but 1000 and 2000 pulses enhanced the current densities. This is likely because as-prepared ci-C already presented enhanced electroactivity (Figure 5a). Figure 5d shows schematic representation comparing the chemical structure of i-C and ci-C coatings. Due

to the high electronegativity of TPP ions, i-C coatings are likely to act as a barrier for anions to permeate and compensate the faradaic reactions in PEDOT. In ci-C coatings, the partial replacement of ionic cross-links with covalent may result in a material more permeable to anions from the electrolyte. This could potentially explain the observed enhancement in electroactivity of the ci-C coating, as shown in Figure 5a. Additionally, the diminished electroactivity of the ox-IPN in the i-C coating, as illustrated in Figure 5b, could be attributed to this effect. Figure 5e illustrates a modified Randles equivalent circuit,^[23,56] where the solution resistance (R_s) models the ionic conductivity of the PBS-supporting electrolyte and the electronic resistance (R_{PEDOT}) is due to electronic charge flow in PEDOT chains. The CPE has the CPE parameter (Y_0) and deviation from ideal capacitance behavior (n). A double-layer capacitance is attributed to the electrolyte ionic compensation of the charges. We fitted EIS spectra from all types of interface to extract values for the putative electronic components in the model (Figure 5f). For both types of IPN functionalization,

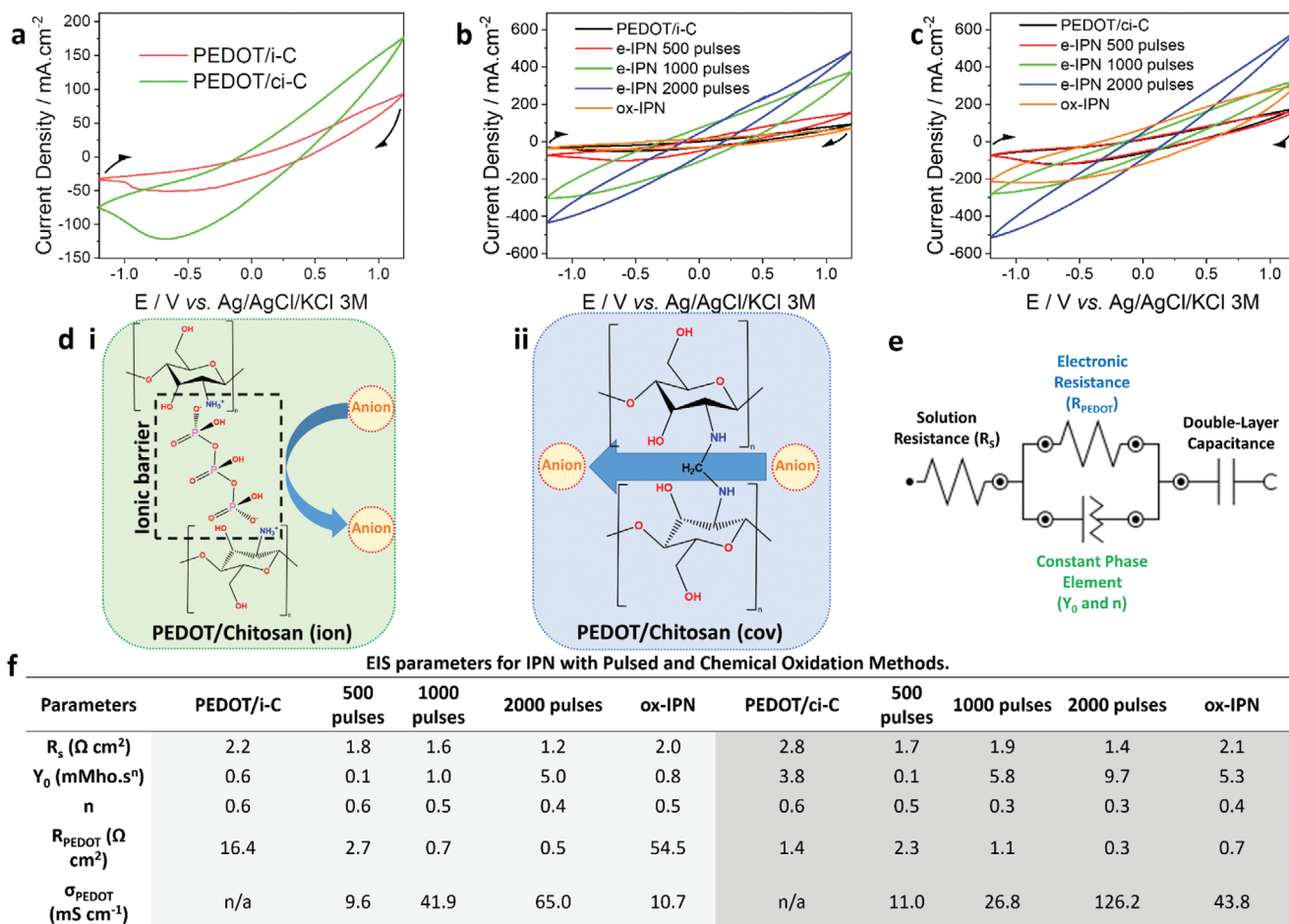


Figure 5. a) CVs of PEDOT/i-C, PEDOT/ci-C. b) IPN functionalization of i-C hydrogels. c) IPN functionalization of ci-C hydrogels. d) Ionic and covalent cross-linking mechanisms are implicated in controlling the ionic conductivity of the chitosan hydrogel. e) Modified Randles equivalent circuit used to model the electrical properties of the interface, R_s indicates solution resistance, R_{PEDOT} is the electronic resistance of PEDOT, constant phase element (CPE) of the hydrogel containing Y_0 as the CPE parameter ($Y\omega^n$), where Y is admittance (reciprocal of the impedance), ω is frequency, and n is the deviation from ideal capacitive behavior; and double-layer capacitance.^[55] f) Table with values for the electronic components in the proposed equivalent circuit. Values were extracted by fitting the circuit to EIS spectra.

we observe a decrease in n , meaning the CPE tends to act more as a resistor than a capacitor. It is in agreement with qualitative observations of CVs where the shape becomes more resistive (i.e., tendency to Ohm's law). The electronic resistance decreases with IPN polymerization inside the hydrogel matrix (with notable exception for i-C coating treated with ox-IPN). The electronic conductivity of samples was calculated from R_{PEDOT} values and considering radial conduction in the samples (Figure S6, Supporting Information). The highest conductivity is achieved for the functionalized hydrogel matrix of ci-C in agreement with the above discussion of Figure 5a,d. It suggests the increase in the amount of PEDOT as the IPN is formed significantly improves conductivity, likely due to higher interconnectivity of pathways for electron flow. We assume a better balance between ionic and electronic conductivity is achieved for PEDOT/i-C with 1000 pulses via e-IPN and PEDOT/ci-C via ox-IPN, with conductivities of 41.9 and 43.8 mS cm⁻¹ with n equals to 0.46 and 0.44, respectively.

The primary focus of this study is to explore the potential of chitosan as a biocompatible and biodegradable material for

bioelectronics and biomedical applications, while harnessing the electrical functionalities of the conducting polymer, PEDOT. The electrochemical properties of several PEDOT/Chitosan materials mentioned in the literature are presented in **Table 1**. We have specifically chosen studies that align with the purpose and properties previously mentioned. It is evident that there are numerous approaches to incorporating PEDOT into hydrogel matrices; however, direct comparisons are challenging due to variations in the reporting of essential electrochemical characterization parameters, such as CV and EIS. Our proposed materials exhibit a higher current density in CV and lower PEDOT resistance compared with previously reported works. Although the conductivity values of our materials are slightly lower than those of PEDOT in chitosan/gelatin-blended matrices, they are considerably higher than those of other proposed materials. In the study conducted by Li and colleagues, the conductivity determined is inconsistent with the current density reported in the CV, suggesting that the 2-probe method used for its determination was not accurate.^[64] The comparative table highlights

Table 1. Current density, PEDOT resistance, and conductivity for PEDOT/chitosan materials.

| Name | Method | Current density | $R_{\text{PEDOT}}^{\text{b)}}$ | Conductivity | Reference |
|--------------------------------|--|---|--------------------------------|---------------------------|-------------------------------|
| Cs–Gel–Agar–2.0% PEDOT: PSS | PEDOT:PSS added to chitosan-gelatin-agar matrix | n/r | n/r | 0.326 mS cm ⁻¹ | Hamzah et al. ^[57] |
| CS-SPVA/PEDOT:PSS hydrogels | Chitosan, starch/cellulose, PVA, and PEDOT:PSS via one-pot synthesis | n/r | n/r | n/r | Remiš et al. ^[54] |
| PEDOT/CMCS (P2) hydrogels | In-situ chemical polymerization of PEDOT in carboxymethyl chitosan (CMCS) | n/r | n/r | 4.68 mS cm ⁻¹ | Sun et al. ^[58] |
| MCS/Gel-0.15EDOT | In-situ chemical polymerization of PEDOT in CMCS/gelatin | n/r | n/r | 1.52 mS cm ⁻¹ | Sun et al. ^[59] |
| ChT-3%PEDOT | Physical mixture of PEDOT nanoparticles with chitin | n/r | n/r | 0.28 mS cm ⁻¹ | Duan et al. ^[60] |
| PEDOT/Cs/Gel scaffolds | In-situ chemical polymerization of PEDOT in chitosan/gelatin | n/r | ≈500 Ω ^{a)} | 76.8 mS cm ⁻¹ | Ma et al. ^[61] |
| 4PEDOT/Cs/Gel | In-situ chemical polymerization of PEDOT in chitosan/gelatin | n/r | n/r | 62.2 mS cm ⁻¹ | Ma et al. ^[62] |
| PC2 | In-situ chemical polymerization of PEDOT:PSS in chitosan/polyvinyl alcohol | 200 μA ^{b)} , 0.1 mM of Ferri-Ferro cyanide + 0.1 mM KCl | n/r | 0.56 mS cm ⁻¹ | Narula et al. ^[63] |
| PDCOH-3 | PEDOT doped with dextran sulfate (DSS) physically mixed with CMCS and gelated with oxidized dextran | 0.6 mA cm ⁻² , PBS | n/r | 2.0 S cm ^{-1c)} | Li et al. ^[64] |
| PEDOT/ci-C | Electrodeposited PEDOT and electro-assisted chitosan hydrogel | 150 mA cm ⁻² , PBS | 1.4 Ω cm ² (17.8 Ω) | - | Present work |
| PEDOT/i-C e-IPN | Electrodeposition of PEDOT (1000 pulses) in i-C matrix | 300 mA cm ⁻² , PBS | 0.7 Ω cm ² (8.9 Ω) | 41.9 mS cm ⁻¹ | Present work |
| PEDOT/ci-C ox-IPN | In-situ chemical polymerization of PEDOT in ci-C matrix | 280 mA cm ⁻² , PBS | 0.7 Ω cm ² (8.9 Ω) | 43.8 mS cm ⁻¹ | Present work |

^{a)} Electrochemical fitting not reported, the value was estimated based on the Nyquist plot; ^{b)} Only current was reported; ^{c)} Conductivity determined using the 2-probe model. The “n/r” is nonreported.

a lack of comprehensive electrochemical characterization for these conductive hydrogel materials.

3. Conclusions

In conclusion, this study presents a novel and effective method for the electro-assisted cross-linking of chitosan hydrogels directly onto organic conductive surfaces. Our approach utilizes the electrochemical release of the cross-linker TPP from a PEDOT surface, enabling the precise and controllable electrical gelation of the chitosan hydrogel. The result is a well-adherent and thick chitosan coating on the electrode surface, ensuring enhanced conductivity, and improved integration. To further enhance the functional properties of the hydrogel coating, we explored postassembly modifications, including covalent cross-linking using formaldehyde and the incorporation of an additional conductive polymer network. Comparative analyses were conducted to evaluate the conductivity enhancement achieved through both electropolymerization and chemical oxidative approaches. Notably, we achieved an optimal balance between ionic and electronic conductivities with ionically cross-linked chitosan coatings modified with an electro-polymerized IPN of PEDOT

(1000 pulses), as well as with covalent-ionic cross-linked chitosan coatings incorporating interpenetrating PEDOT assembled through the oxidative method. The significant outcomes of this research offer valuable insights into the design and development of better conductive hydrogel coatings for soft electronics, showcasing immense potential in various applications, such as wearable sensors and implantable medical electrodes. By successfully achieving the direct growth of chitosan hydrogel onto PEDOT through the electrochemical–chemical (EC) mechanism, we have demonstrated a promising pathway for precise control over the electro-assisted assembly of these materials, leading to superior electrochemical performance compared with previously reported PEDOT/chitosan systems. The reported method adds to a growing list of promising approaches for the functionalization of electrodes with soft and conductive coatings for achieving improved bioelectronic interfaces.

4. Experimental Section

Materials: The chemical reagents 3,4-ethylenedioxythiophene (EDOT), high molecular-weight chitosan (310–375 kDa), sodium chloride, acetic acid, ammonium persulfate (APS), mineral oil, sodium TPP, formaldehyde solution (37% m/m), hexane, and sodium dodecyl sulfate

(SDS) were purchased from Sigma-Aldrich. All solutions were prepared with deionized Milli-Q water (18.2 M Ω) or with PBS pH 7.4 (Gibco).

PEDOT/Chitosan Presolutions: The solution composition was adapted from a previous work.^{17,23} For the PEDOT:TPP, 150 mM of TPP, 70 mM of SDS (ten times critical micellar concentration), and 50 mM of EDOT is dissolved in 24.3 mL of deionized water. For the electro-assisted cross-linking: 1% (v/v) of acetic acid was diluted in 24.3 mL of deionized water, followed by the dissolution of 150 mM of sodium chloride. Later, 1% (m/v) of high molecular-weight chitosan was dissolved under strong stirring for 30 min at room temperature. For covalently cross-linking functionalization, diluted formaldehyde solution (20 wt%) in deionized water was applied. For IPN functionalization via electropolymerization: 70 mM of SDS and 50 mM of EDOT were dissolved in 1 M HCl with total volume of 24.3 mL. For IPN functionalization via chemical oxidative reaction: the first solution was 400 mM of APS dissolved in 1 M of HCl. Second solution was 400 mM of EDOT dissolved in mineral oil.

Preparation of PEDOT/Chitosan Hydrogels: For the PEDOT doped with TPP (PEDOT:TPP), the open-circuit potential interpulse (OCPI)-pulsed protocol was adapted from the previous work to obtain a highly doped conducting polymer.¹⁷ Briefly, the pulse sequence was programmed with 20 s of OCP + loop (number of desired pulses) containing CA at electropolymerization potential (+1.2 V) for 0.5 and 5 s at OCP + 20 s of OCP at the end. For electro-assisted cross-linking of PEDOT/chitosan ionically cross-linked (PEDOT/i-C), it was applied -1.2 V (vs Ag/AgCl/KCl 3 M) for 600 s. For covalently cross-linking functionalization (ci-C), the gold wire coated with PEDOT/i-C was placed in diluted formaldehyde solution for 1 h at room temperature. For the IPN functionalization via electropolymerization (e-IPN), it was applied +1.6 V for 0.5 s and waiting 20 s at the OCP in the OCPI protocol for the number of pulses determined in the loop (500, 1000, or 2000). For the IPN functionalization via chemical oxidative (ox-IPN), the hydrogel was soaked in solution containing APS and HCl for 3 h, followed by dipping into 400 mM EDOT in mineral oil for 6 h. Later, hydrogels were washed in mineral oil overnight. Afterward, the hydrogels were washed in hexane for 1 h and kept in PBS for at least 24 h prior to use.

Scanning Electron Microscopy-Energy Dispersive X-Ray Spectroscopy (SEM-EDS): A Philips/FEI XL-20 SEM (Philips, UK) scanning electron microscope was used to image-dehydrated hydrogel samples. Cross-sections were obtained by first applying the removal procedure of the hydrogel (Figure S3, Supporting Information) and later cutting the hydrogels using a razor blade when freshly prepared. The samples were dehydrated by replacing water with ethanol, kept overnight in ethanol solution, and afterward processed in a critical point dryer (CPD). Samples were placed in SEM stubs over carbon tape in vertical position and sputter coated with gold before SEM imaging. The gold-coated dried hydrogels were then imaged with an accelerating voltage of 10 kV.

Electrochemical Measurements: CV, CA, and EIS were performed using a potentiostat/galvanostat (PARSTAT3000, AMETEK) controlled using VersaStudio 2.60.2 software. CVs were recorded in PBS media as supporting electrolyte, from -1.2 to +1.2 V using scan rate of 100 mV s⁻¹. EIS were recorded from 1 MHz to 0.1 Hz, with excitation amplitude of 10 mV (RMS) at ten points per decade for full spectra. The employed was gold wire with submersed length in solution of either 1 or 0.5 inch (1.27–2.54 cm). The 1-inch long wire was used for mechanical integrity check (Figures S3 and S7, Supporting Information), while the 0.5-inch wire was used for all other experiments. The area of the gold electrode was determined as 0.04 cm². A commercially available Ag/AgCl/KCl 3 M (BASi) electrode and a platinum wire coiled were used as reference and counter electrodes, respectively. For statistical analysis, all experiments were made in triplicate using three different gold wire electrodes and freshly prepared solutions. Unless stated otherwise, data were reported as the mean \pm standard deviation. Parameter fitting and circuit simulation was conducted using the NOVA 2.1 software (Metrohm Autolab). All charges were calculated by $Q = \int_{t_i}^{t_f} I dt$, where I is the current density (A cm⁻²) and t is time (seconds). The electronic conductivity (σ_{PEDOT}) was calculated using the equation in Figure S6 (Supporting Information).

Supporting Information

Supporting Information is available from the Wiley Online Library or from the author.

Acknowledgements

All the authors acknowledge SURE scheme and Insigneo for the student's scholarships and funding from ERC Starting grant No.: IntegraBrain (804005).

Conflict of Interest

The authors declare no conflict of interest.

Author Contributions

A.C.Da.S.: Conceptualization, Methodology, Formal analysis, Resources, Writing—Original Draft, Writing—Review & Editing, Supervision. C.A.-D.: Investigation, Formal analysis, Data Curation. S.K.: Investigation, Formal analysis, Data Curation. J.D.: Investigation, Formal analysis, Data Curation. R.K.K.C.: Investigation, Formal analysis, Data Curation. T.E.P.: Writing—Review & Editing, Supervision. I.R.M.: Writing—Review & Editing, Supervision, Project administration, Funding acquisition.

Data Availability Statement

The data that support the findings of this study are available from the corresponding author upon reasonable request.

Keywords

bioelectronics, chitosan, electrochemically driven assembly, hydrogels, PEDOT surfaces

Received: August 1, 2023

Published online:

- [1] H. Yuk, J. Wu, X. Zhao, *Nat. Rev. Mater.* **2022**, 7, 935.
- [2] I. R. Minev, *J. Polym. Sci.* **2023**, 61, 1707.
- [3] Q. Liang, Z. Shen, X. Sun, D. Yu, K. Liu, S. M. Mugo, W. Chen, D. Wang, Q. Zhang, *Adv. Mater.* **2023**, 35, 2211159.
- [4] M. Shur, O. Akouissi, O. Rizzo, D. J. Colin, J. M. Kolinski, S. P. Lacour, *Biomaterials* **2023**, 294, 122024.
- [5] M. Shur, F. Fallegger, E. Pirondini, A. Roux, A. Bichat, Q. Barraud, G. Courtine, S. P. Lacour, *ACS Appl. Bio. Mater.* **2020**, 3, 4388.
- [6] H. Zhou, T. Li, Y. Y. Duan, *Sens. Actuators B Chem.* **2012**, 161, 198.
- [7] A. C. Da Silva, T. E. Paterson, I. R. Minev, *Soft Sci.* **2023**, 3, 3.
- [8] R. T. Hassarati, W. F. Dueck, C. Tasche, P. M. Carter, L. A. Poole-Warren, R. A. Green, *IEEE Trans. Neural Syst. Rehabil. Eng.* **2014**, 22, 411.
- [9] J. O. Winter, S. F. Cogan, J. F. Rizzo, *J. Biomed. Mater. Res., Part B* **2007**, 81B, 551.
- [10] C. Kleber, K. Lienkamp, J. R uhe, M. Asplund, *Adv. Healthcare Mater.* **2019**, 8, 1801488.
- [11] R. Portillo-Lara, J. A. Goding, R. A. Green, *Curr. Opin. Biotechnol.* **2021**, 72, 62.

- [12] U. A. Aregueta-Robles, P. J. Martens, L. A. Poole-Warren, R. A. Green, *J. Polym. Sci., Part B: Polym. Phys.* **2018**, *56*, 273.
- [13] H. Yuk, B. Lu, X. Zhao, *Chem. Soc. Rev.* **2019**, *48*, 1642.
- [14] J. i. Liu, S. Lin, X. Liu, Z. Qin, Y. Yang, J. Zang, X. Zhao, *Nat. Commun.* **2020**, *11*, 1071.
- [15] H. Yuk, T. Zhang, S. Lin, G. A. Parada, X. Zhao, *Nat. Mater.* **2016**, *15*, 190.
- [16] R. Takahashi, K. Shimano, H. Okazaki, T. Kurokawa, T. Nakajima, T. Nonoyama, D. R. King, J. P. Gong, *Adv. Mater. Interfaces* **2018**, *5*, 1801018.
- [17] G. A. Parada, H. Yuk, X. Liu, A. J. Hsieh, X. Zhao, *Adv. Healthcare Mater.* **2017**, *6*, 1700520.
- [18] Y. i. Cheng, X. Luo, J. Betz, G. F. Payne, W. E. Bentley, G. W. Rubloff, *Soft Matter* **2011**, *7*, 5677.
- [19] M. Lei, X. Qu, H. Wan, D. Jin, S. Wang, Z. Zhao, M. Yin, G. F. Payne, C. Liu, *Sci. Adv.* **2022**, *8*, 15.
- [20] J. Li, E. Kim, K. M. Gray, C. Conrad, C.-Y. u Tsao, S. P. Wang, G. Zong, G. Scarcelli, K. M. Stroka, L.-X. i Wang, W. E. Bentley, G. F. Payne, *Adv. Funct. Mater.* **2020**, *30*, 2001776.
- [21] Y. Wang, Y. i. Liu, Y. i. Cheng, E. Kim, G. W. Rubloff, W. E. Bentley, G. F. Payne, *Adv. Mater.* **2011**, *23*, 5817.
- [22] V. R. Feig, H. Tran, M. Lee, K. Liu, Z. Huang, L. Beker, D. G. Mackanic, Z. Bao, *Adv. Mater.* **2019**, *31*, 1902869.
- [23] A. C. Da Silva, J. Wang, I. R. Minev, *Nat. Commun.* **2022**, *13*, 1353.
- [24] J. Stejskal, *Chem. Pap.* **2017**, *71*, 269.
- [25] C. M. Tringides, N. Vachicouras, I. De Lázaro, H. Wang, A. Trouillet, B. o R. i Seo, A. Elosegui-Artola, F. Fallegger, Y. Shin, C. Casiraghi, K. Kostarelos, S. P. Lacour, D. J. Mooney, *Nat. Nanotechnol.* **2021**, *16*, 1019.
- [26] C. M. Tringides, M. Boulingre, A. Khalil, T. Lungjangwa, R. Jaenisch, D. J. Mooney, *Adv. Healthcare Mater.* **2022**, *12*, 16.
- [27] H. Yuk, B. Lu, S. Lin, K. Qu, J. Xu, J. Luo, X. Zhao, *Nat. Commun.* **2020**, *11*, 1604.
- [28] M. Solazzo, K. Krukiewicz, A. Zhussupbekova, K. Fleischer, M. J. Biggs, M. G. Monaghan, *J. Mater. Chem. B* **2019**, *7*, 4811.
- [29] A. C. Da Silva, V. H. Paschoal, M. C. C. Ribeiro, S. I. C. de Torresi, *Macromol. Chem. Phys.* **2022**, *223*, 2200275.
- [30] V. R. Feig, H. Tran, M. Lee, Z. Bao, *Nat. Commun.* **2018**, *9*, 2740.
- [31] J. Goding, A. Gilmour, P. Martens, L. Poole-Warren, R. Green, *Adv. Healthcare Mater.* **2017**, *6*, 1601177.
- [32] C. Tondera, T. F. Akbar, A. K. Thomas, W. Lin, C. Werner, V. Busskamp, Y. Zhang, I. R. Minev, *Small* **2019**, *15*, 1901406.
- [33] Y. Yang, L. Xu, J. Wang, Q. Meng, S. Zhong, Y. Gao, X. Cui, *Carbohydr. Polym.* **2022**, *283*, 119161.
- [34] S. i. Wu, S. Wu, X. Zhang, T. Feng, L. Wu, *Biosensors* **2023**, *13*, 93.
- [35] B. Tian, S. Hua, Y. u. Tian, J. Liu, *J. Mater. Chem. B* **2020**, *8*, 10050.
- [36] H. Hamedi, S. Moradi, S. M. Hudson, A. E. Tonelli, *Carbohydr. Polym.* **2018**, *199*, 445.
- [37] M. Jia, J. Kim, T. Nguyen, T. Duong, M. Rolandi, *Biopolymers* **2021**, *112*, 15.
- [38] J. Berger, M. Reist, J. M. Mayer, O. Felt, N. A. Peppas, R. Gurny, *Eur. J. Pharm. Biopharm.* **2004**, *57*, 19.
- [39] J. Berger, M. Reist, J. M. Mayer, O. Felt, R. Gurny, *Eur. J. Pharm. Biopharm.* **2004**, *57*, 35.
- [40] D. Elieh-Ali-Komi, M. R. Hamblin, *Int. J. Adv. Res.* **2016**, *4*, 411.
- [41] L. Racine, I. Texier, R. Auzély-Velty, *Polym. Int.* **2017**, *66*, 981.
- [42] K. Ravishankar, R. Dhamodharan, *React. Funct. Polym.* **2020**, *149*, 104517.
- [43] A. F. Martins, D. M. De Oliveira, A. G. B. Pereira, A. F. Rubira, E. C. Muniz, *Int. J. Biol. Macromol.* **2012**, *51*, 1127.
- [44] S. Sreekumar, F. M. Goycoolea, B. M. Moerschbacher, G. R. Rivera-Rodriguez, *Sci. Rep.* **2018**, *8*, 4695.
- [45] C. Pan, J. Qian, C. Zhao, H. Yang, X. Zhao, H. Guo, *Carbohydr. Polym.* **2020**, *241*, 116349.
- [46] D. R. Bhumkar, V. B. Pokharkar, *AAPS PharmSciTech* **2006**, *7*, E138.
- [47] F. Khoerunnisa, M. Nurhayati, F. Dara, R. Rizki, M. Nasir, H. A. Aziz, H. Hendrawan, N. E. Poh, C. Kaewsaneha, P. Opaprakasit, *Fibers Polym.* **2021**, *22*, 2954.
- [48] A. M. Dos Santos, S. G. Carvalho, L. M. B. Ferreira, M. Chorilli, M. P. D. Gremião, *Colloids Surfaces A Physicochem. Eng. Asp.* **2022**, *640*, 128417.
- [49] Q. Ta, J. Ting, S. Harwood, N. Browning, A. Simm, K. Ross, I. Olier, R. Al-Kassas, *Eur. J. Pharm. Sci.* **2021**, *160*, 105765.
- [50] P. Huang, C. Huang, X. Ma, C. Gao, F. Sun, N. Yang, K. Nishinari, *Food Hydrocoll.* **2021**, *121*, 106972.
- [51] B. Yuan, C. Li, Y. Zhao, O. Gröning, X. Zhou, P. Zhang, D. Guan, Y. Li, H. Zheng, C. Liu, Y. Mai, P. Liu, W. Ji, J. Jia, S. Wang, *J. Am. Chem. Soc.* **2020**, *142*, 10034.
- [52] S. Laishevskina, N. Shevchenko, O. Iakobson, A. Dobrodumov, V. Chelibanov, E. Tomšik, *Molecules* **2022**, *27*, 7576.
- [53] S. Wang, S. Guan, Z. Zhu, W. Li, T. Liu, X. Ma, *Mater. Sci. Eng. C* **2017**, *71*, 308.
- [54] J. M. Dodda, M. G. Azar, P. Belský, M. Slouf, A. Broz, L. Bačáková, J. Kadlec, T. Remiš, *Cellulose* **2022**, *29*, 6697.
- [55] P. Charoen-Amornkitt, T. Suzuki, S. Tsushima, *Electrochemistry* **2019**, *87*, 204.
- [56] T. Shay, O. D. Velev, M. D. Dickey, *Soft Matter* **2018**, *14*, 3296.
- [57] D. A. Ahmad Ruzaidi, M. M. Mahat, Z. Mohamed Sofian, N. A. Nor Hashim, H. Osman, M. A. Nawawi, R. Ramli, K. A. Jantan, M. F. Aizamuddin, H. H. Azman, Y. H. Robin Chang, H. H. Hamzah, *Polymers* **2021**, *13*, 2901.
- [58] C. Xu, S. Guan, S. Wang, W. Gong, T. Liu, X. Ma, C. Sun, *Mater. Sci. Eng. C* **2018**, *84*, 32.
- [59] S. Guan, Y. Wang, F. Xie, S. Wang, W. Xu, J. Xu, C. Sun, *Molecules* **2022**, *27*, 8326.
- [60] L. Huang, X. Yang, L. Deng, D. Ying, A. Lu, L. Zhang, A. Yu, B. Duan, *ACS Appl. Mater. Interfaces* **2021**, *13*, 16106.
- [61] S. Wang, S. Guan, W. Li, D. Ge, J. Xu, C. Sun, T. Liu, X. Ma, *Mater. Sci. Eng. C* **2018**, *93*, 890.
- [62] S. Wang, C. Sun, S. Guan, W. Li, J. Xu, D. Ge, M. Zhuang, T. Liu, X. Ma, *J. Mater. Chem. B* **2017**, *5*, 4774.
- [63] S. Khan, A. K. Narula, *Eur. Polym. J.* **2016**, *81*, 161.
- [64] C. Yu, Z. Yue, H. Zhang, M. Shi, M. Yao, Q. Yu, M. Liu, B. Guo, H. Zhang, L. Tian, H. Sun, F. Yao, J. Li, *Adv. Funct. Mater.* **2023**, *33*, 15.